Chapter 20
Properties of 63Sn-37Pb and Sn-3.8Ag-0.7Cu Solders Reinforced with Single-Wall Carbon Nanotubes

K. Mohan Kumar, Vaidyanathan Kripesh, and Andrew A. O. Tay

20.1 Introduction

As integrated circuit (IC) technology continues to advance, there will be increasing demands on I/O counts and power requirements, leading to decreasing solder pitch and increasing current density for solder balls in high-density wafer-level packages [1]. As the electronics industry continues to push for miniaturization, reliability becomes a vital issue. The demand for more and smaller solder bumps, while increasing the current, has also resulted in a significant increase in current density [2] which can cause the failure of solder interconnects due to electromigration [3].

Solders are extensively used in IC technology as mechanical and electrical interconnects because of their ease of processing and lower cost. However, because of their relatively low melting temperatures, creep is a major concern. When electronic devices are switched on and off, the electronic packages experience cyclic changes in temperature. Due to differences between the packages and the substrate, cyclic changes in thermomechanical stresses are induced in the package-to-board solder joints. Such cyclic stresses in the solder joints eventually lead to failure of the solder joints through thermomechanical fatigue [4, 5].

With the relentless trend toward very fine-pitch IC packages, the cyclic stresses experienced by flip chip-to-board interconnects are increasing greatly resulting in a drastic drop in fatigue life of solder joints. One way of overcoming this problem is to

K. Mohan Kumar
Department of Mechanical Engineering, Raghu Engineering College, Andhrapradesh, India

V. Kripesh
Institute of Technical Education, Singapore, Singapore

A. A. O. Tay (✉)
Singapore University of Technology and Design and Central South University, Changsha, Hunan, China
e-mail: andrew_tay@ieee.org

© Springer International Publishing AG, part of Springer Nature 2018

J. E. Morris (ed.), *Nanopackaging*, https://doi.org/10.1007/978-3-319-90362-0_20

use new materials which can provide enhanced mechanical, electrical, and thermal properties. Composite solders can offer improved properties [6]. Although a few researchers have investigated the influence of nanoparticles and nanotubes influence on the properties of solder [7–9], these investigators were mainly focused on the mechanical properties of the solders. In this study, the influence of nanotube addition on microstructural, mechanical, electrical, wetting, and thermal properties has been investigated. In addition to this, efforts have been made to evaluate the joint strength and creep strength of the composite solder joints.

Owing to their fascinating physical properties and unique structures, carbon nanotubes (CNTs) are receiving steadily increasing attention since their discovery [10]. Intense interest from researchers has been generated in utilizing these unique structures and outstanding properties, for example, in hydrogen storage, supercapacitors, biosensors, electromechanical actuators, nanoprobes for high-resolution imaging, and so on [11, 12]. In recent years, there has been a steadily increasing interest in the development of CNT-reinforced composites due to their remarkable mechanical, electrical, and thermal properties [13–16]. Depending on their length, diameter, chirality, and orientations, CNTs show almost five times the elastic modulus (1 TPa) and nearly 100 times the tensile strength (150 GPa) of high strength steels [17]. The motive is to transfer the exceptional mechanical and physical properties of carbon nanotubes to the bulk engineering materials. Polymers, ceramics, and metal are favorable as matrix materials. CNT-reinforced polymer-based composites were widely synthesized by surfactant-assisted processing, repeated stirring, solution evaporation with high energy sonication, and interfacial covalent functionalization [18–20]. Much of the research in nanotube-based composites has been on polymer or ceramic matrix materials and less on metal matrix composites [21–23]. This is mainly due to the fact that uniform dispersion of CNTs in a metal matrix is quite difficult.

Nai et al. [9] demonstrated that the dispersion and homogenous mixing between MWCNTs and a lead-free solder matrix could be obtained by mixing nano-sized matrix powders with CNTs. They showed that the powder metallurgy process was a very promising technique for full densification of CNT/lead-free solder nanocomposites which showed remarkable enhancement of yield strength compared to that of unreinforced lead-free solders.

The current work provides an insight into the usage of SWCNTs as a reinforcing material for the enhancement of the solder material properties to be used in wafer-level chip-scale packages (WLCSP). The aim of this work is to fabricate and characterize CNT-reinforced nanocomposite solders and show their improved physical, thermal, electrical, mechanical, and wetting properties compared to the original Sn-Pb and Sn-Ag-Cu solders.

20.2 Experimental Aspects

20.2.1 Materials

The starting materials used in this study were Sn-Pb and Sn-Ag-Cu solder powders of Type 7 (2–11 μm). The SWCNTs employed in this study were prepared using the chemical vapor deposition technique and typically have an average diameter of 1.2 nm and lengths between 5 and 10 μm.

20.2.2 Preparation of Composite Solders

The solder powder and SWCNTs were weighed to the approximate weight % ratio. Different compositions were prepared with varying SWCNT content ranging from 0.01 to 1 wt%. The pre-weighed SWCNTs and solder powders were blended homogeneously using a V-cone blender operated at a speed of 50 rpm. The homogenously blended composite solder powders were consolidated by uniaxial cold pressing with a pressure of 110 bar in the case of Sn-Pb composite solders, while Sn-Ag-Cu composite solders were compacted at a pressure of 120 bar. The consolidated "green" composite solder compacts of diameter 35 mm were sintered at 150 °C for Sn-Pb composite solders and at 180 °C for Sn-Ag-Cu composite solders to approach a reasonable rate of solid state sintering. The sintered compacts were finally extruded at room temperature with an extrusion ratio of 20:1.

20.2.3 Scanning Electron Microscopy

Samples were cut from the extruded solder bars with a diamond saw and mechanically polished with diamond pastes after cutting, finishing with 0.02 μm grade. Microstructural observations were performed by scanning electron microscopy using a Hitachi FE-SEM 4100 operated at 10 kV. The elemental analysis of the phases was carried out using energy-dispersive X-ray spectroscopy (EDX) equipped with FE-SEM.

20.2.4 Thermomechanical Analysis (TMA)

The linear thermal expansion coefficient of composite solders was measured using a Perkin-Elmer TMA-7 thermal mechanical analyzer operated in expansion mode. Cylindrical samples of diameter 8 mm were employed. TMA data were obtained in the heating range of 25–125 °C in the case of Sn-Pb composite solders, while a

25–150 °C heating range was employed for the Sn-Ag-Cu composite solders at a rate of 5 °C/min. All TMA experiments were performed with a small loading force of 5 g to avoid deformation of the samples during testing. The CTEs of the composite solder specimens were obtained from the slope of the curve over a linear temperature range.

20.2.5 Differential Scanning Calorimetry (DSC)

The melting behaviors of the composite solder specimens were examined by a Perkin-Elmer DSC-7 system. DSC experiments were carried out at a heating rate of 10 °C/min from 25 to 250 °C. The heat flow as a function of temperature was recorded and analyzed. The entire scanning was carried out under an inert nitrogen atmosphere.

20.2.6 Electrical Properties

Electrical conductivity was measured on strips having dimensions of 50 × 10 mm cut from rolled composite solder preforms with a thickness of approximately 0.13 mm using a four-point probe technique.

20.2.7 Wettability

Solder alloys were cold rolled to preforms of thickness 1 mm and 0.13 mm for the joint tensile testing, wetting, and creep rupture analyses. The solder preforms were remelted four times in order to get a uniform structure and composition. Approximately 0.2 g of the remelted solder preforms were weighed using an electronic balance. The weighed solder preforms were cleaned with acetone in an ultrasonic bath. The substrate used was a thin copper plate of 99.9% purity and dimensions of 25 × 25 × 0.1 mm. These small substrates were polished sequentially with silicon carbide sandpaper of up to 800 abrasive number and then cleaned ultrasonically in acetone for 10 min to achieve an ultraclean substrate for wetting experiments.

The measurement of contact angle was performed using the following technique. First wetting was carried out on a hot plate. Rosin mildly activated (RMA) flux was applied on a copper substrate. Some flux was then applied on the surface of the pre-weighed solder preform before placing it on the copper substrate. In preparation for the reflow, the substrate containing the solder and the flux was first preheated to 100 °C and then to the reflow temperature of 240 °C. After the time of reflow, the specimen was quickly removed, allowed to solidify, and later quenched to room temperature. The solder after reflow on the copper substrate was cleaned with

alcohol for 10 min to remove the flux residues. After each test, the solder drop was cut perpendicular to the interface, mounted in resin, and polished to examine the morphology and contact angle of solder on copper substrate. Then the photograph of the specimen was taken and analyzed with the help of commercially available software for measuring the spreading area.

20.2.8 Microhardness Testing

The sintered samples were polished to a mirror finish prior to the microhardness indentation tests. Microhardness of the composite solder specimens were measured using a Digital Micro-Hardness Tester with a Vickers indenter. The samples were indented with a load of 10 g, and an average of seven indentations was made at different locations of the composite solder specimens for further analysis.

20.2.9 Tensile Testing

The samples for tensile testing were machined from the extruded bars. Dog-bone-shaped specimens of gauge length 25 mm and diameter 5 mm were prepared. Tensile experiments were carried out at room temperature on the specimens using an Instron 5569 tensile tester at a constant cross-head displacement of 1 mm/min. Five samples of each composite solder were tested. All samples were tested to failure.

20.2.10 Tensile Strength of Solder Joint

Cu samples of length 45 mm were cut from a 99.9% pure, half-hardened Cu bar with rectangular cross section (10 × 1 mm). These were etched in 50% sulfuric acid to get rid of the surface oxide layer. The mating surfaces were fluxed immediately with commercial RMA flux, and the rest of the surfaces were coated with solder resist to prevent them from being wetted by molten solder. Solder alloys were rolled into thin sheets of thickness 1 mm and sliced into pieces that approximately covered the mating surface area of the Cu samples. Then, the sliced solder pieces were placed between the mating surfaces of two Cu samples in an aluminum mold and were heated in a furnace to a temperature 50 °C above the liquidus of the solder. After holding in the molten state for 2 min, the samples were gently soldered with the help of a screw-driven mold to maintain a joint thickness of 500 μm by adjusting the screws placed at each end of the mold to obtain a good joint and were cooled in the furnace. It was found that the tensile testing specimens thus prepared resulted in joints with solder of thickness of between 300 and 400 μm.

20.2.11 Creep Rupture Analysis

The creep rupture tests were conducted using composite solder lap joints between two dog-bone-shaped copper pieces which were fabricated as follows. Two 99.9% pure, 0.1 mm thin copper sheets were first wire cut into the shape of a dog bone. The composite solder alloys were cold rolled to obtain performs of thickness 0.13 mm and cut into square specimens of dimensions 1×1 mm. The dog-bone-shaped copper substrates were cleaned with dilute sulfuric acid and rinsed with acetone. The narrow ends of the copper substrates were coated with solder resist to obtain a cross-sectional area of 1 mm^2. Then, RMA flux was applied to each narrow end of the substrate, and the composite solder preform was sandwiched between the two copper substrates. Reflow soldering was performed in a programmable oven. The creep rupture life tests were performed at room temperature with a dead load stress of approximately 10.4 MPa.

20.3 Results and Discussion

20.3.1 Microstructural Observation

The SEM and TEM microstructures of the as-received SWCNTs used in the present study are shown in Fig. 20.1. The FE-SEM microstructure of the original Sn-Pb solder is shown in Fig. 20.2a showing white contrast for tin grains and dark contrast for lead grains. The average grain size of the as-cast Sn-Pb solder was 5.12 μm. Figure 20.2b shows the highly refined microstructure of 0.3 wt% SWCNT-doped Sn-Pb composite solder, which is a consequence of homogenous dispersion of the

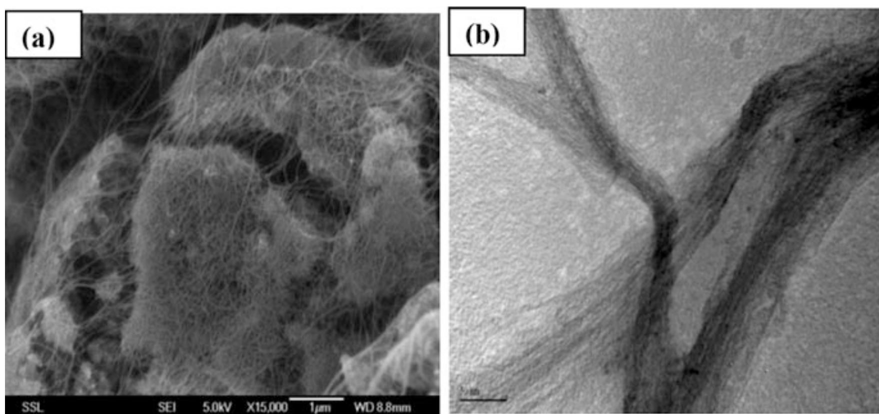

Fig. 20.1 Images of SWCNTs: (**a**) SEM image of SWCNT, (**b**) TEM micrograph of SWCNT produced by a CVD process

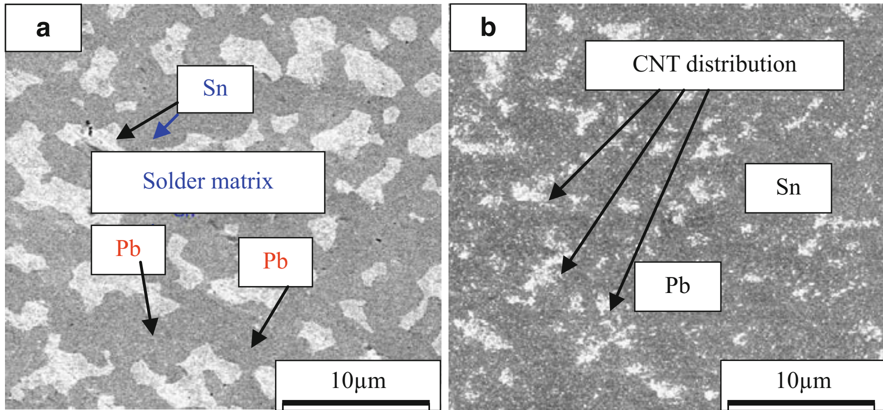

Fig. 20.2 FE-SEM micrographs of 63Sn-37Pb solder with (**a**) 0 wt% SWCNT, (**b**) 0.3 wt% SWCNT

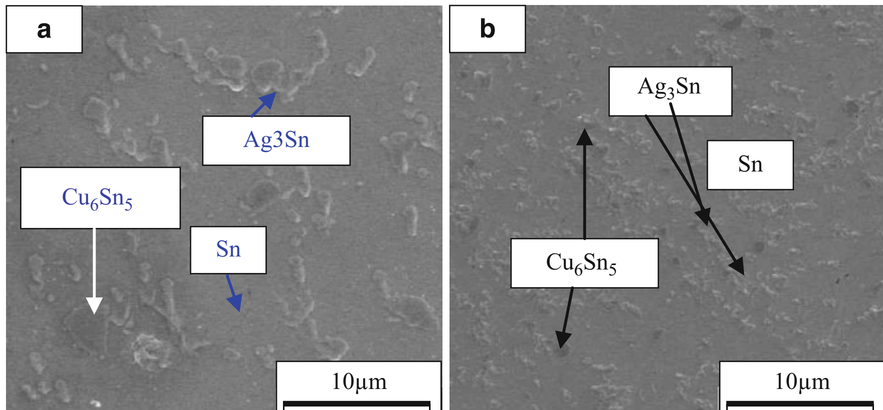

Fig. 20.3 FE-SEM micrographs of Sn-3.8Ag-0.7Cu with (**a**) 0 wt% SWCNT, (**b**) 1 wt% SWCNT

nanotubes. The average grain size of the composite is measured to be 1.08 μm by employing image analysis software. An obvious difference between the microstructures of the solder alloys with and without addition of nanotubes can be observed.

There is some porosity observed in the solder matrix. This is mainly attributed to the sintering process. During the sintering process, the matter of the solder matrix flows and the SWCNTs act as solid impurities [24]. The van der Waal forces cause the SWCNTs to get entangled with one another. Because of this phenomenon, it is very difficult to achieve a higher degree of homogeneous dispersion of the SWCNTs throughout the solder matrix. In this manner the entangled SWCNTs may have resulted in the formation of pores in the solder matrix which is being observed in the micrographs.

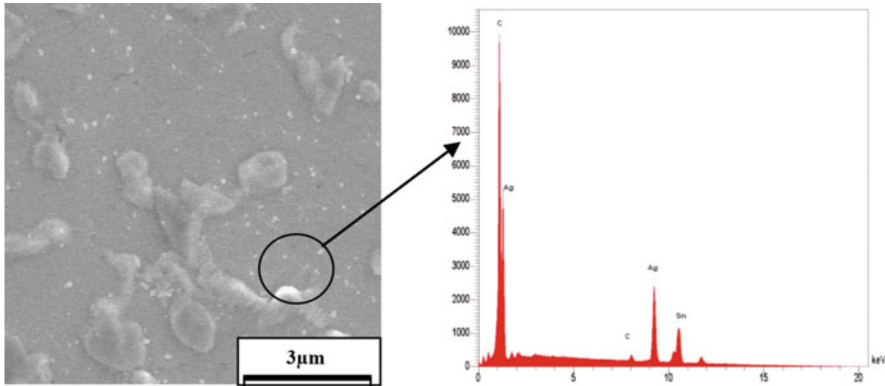

Fig. 20.4 Phase identification of SWCNT at the grain boundary of Ag_3Sn in sintered Sn-Ag-Cu/CNT composite: EDS of the white region showing the presence of carbon

Figure 20.3 compares the microstructures of the Sn-Ag-Cu + SWCNT composite solders and pure Sn-Ag-Cu solder. The higher magnification micrographs in Fig. 20.3a reveal that the microstructure of Sn-Ag-Cu solder is composed of a dark gray phase (Cu_6Sn_5) and brighter light gray grains (Ag_3Sn) dispersed evenly in the β-Sn solder matrix. For the Sn-Ag-Cu pure solder sample, the average grain size of the secondary phase varied between 3.75 μm and 4.25 μm. The average grain size of the secondary phase was found to be 0.5–0.8 μm with 1 wt% addition of nanotubes to the Sn-Ag-Cu solder as shown in Fig. 20.3b. In the SWCNT-reinforced solder samples, the SWCNTs are distributed at the boundaries of the Ag_3Sn equiaxed grains. They can be identified by the difference in contrast, which is mainly associated with the different atomic numbers of the individual phases under consideration. Brighter regions correspond to the higher atomic numbers, while darker phases correspond to the lower atomic numbers. The elemental analysis obtained by EDX is shown in Fig. 20.4. The intense "C" peak represents the presence of SWCNTs at the boundaries of the Ag_3Sn grains. This shows that the SWCNTs remained inside the solder matrix after sintering but were concentrated at the boundaries of the Ag_3Sn grains.

The possible reason for the size refinement is as follows. SWCNT is a ceramic material. While processing the composite solder specimens, the surface diffusion of the Ag_3Sn can be suppressed by the extremely quick translations of ceramic materials through the temperatures that exist during the sintering process [25]. The reinforcement of the microstructure, as shown in Fig. 20.2 with the varying content of SWCNT, demonstrates a strong dependence of the sintered microstructure of the composite solders on the initial composition and morphology of the starting materials.

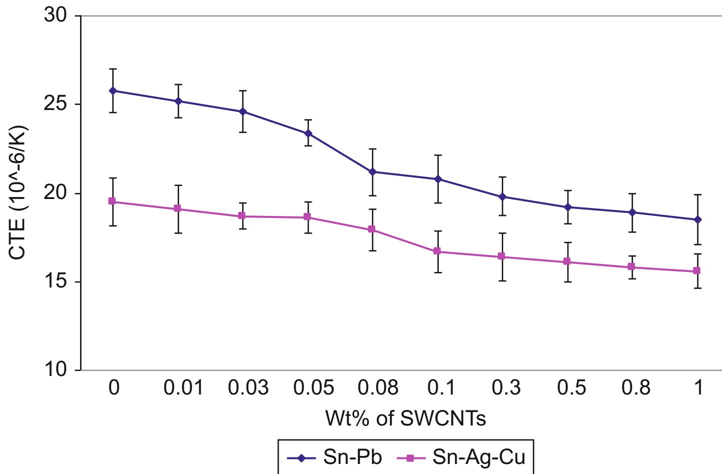

Fig. 20.5 Variation of CTE of both Sn-Pb and Sn-Ag-Cu composites with wt% of SWCNTs

Table 20.1 Onset and melting temperatures of Sn-Pb and Sn-Ag-Cu composite solders

	63Sn-37Pb		Sn-3.8Ag-0.7Cu	
Wt% SWCNT	Onset temp (°C)	Melting temp (°C)	Onset temp (°C)	Melting temp (°C)
0	181.1	183.3	217.7	221.0
0.03	181.1	182.8	217.1	220.1
0.08	180.2	182.2	216.4	219.8
0.1	179.5	182.0	216	219.3
0.3	179	181.9	215.6	218.9
1	176.3	181.1	213.4	217.9

20.3.2 Coefficient of Thermal Expansion (CTE)

The CTE was measured using TMA and was obtained from the initial linear slope of the thermal strain-temperature plot. The CTEs of pure Sn-Pb and Sn-Ag-Cu were found to be 25.8×10^{-6}/°C and 18.7×10^{-6}/°C, respectively, which are comparable with those in the literature [26, 27]. The variation of CTE with wt% of SWCNT addition, for the Sn-Pb and Sn-Ag-Cu composites, is shown in Fig. 20.5. The composite solders exhibit lower CTE values than the parent alloys. It was observed that the CTE of both the solders decreases with increasing content of SWCNT. In general, the lower CTE can be attributed to the rigidity of the nanotubes and the fine dispersion of nanotubes in the solder matrix, which can obstruct the expansion of the solder matrix at elevated temperatures. However, factors such as the adhesion of nanotube-matrix interfaces at testing temperatures, the apparent lack of orientation of the nanotubes, and the inevitable agglomeration at higher nanotube loads might affect the CTE values of nanocomposite solders and need to be confirmed by further studies and analysis.

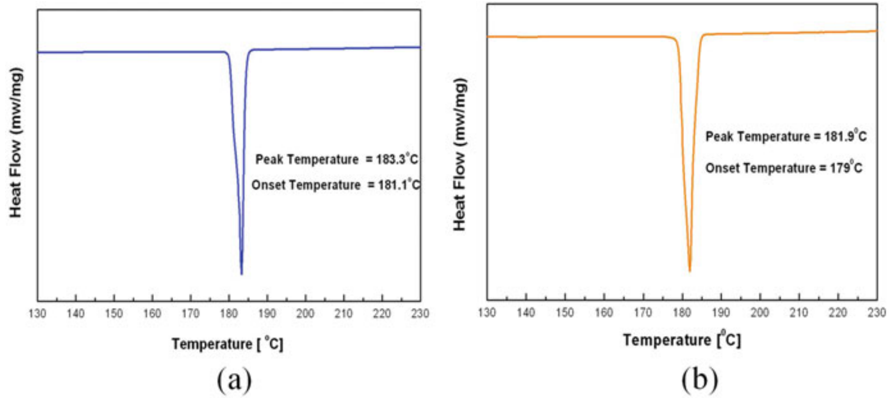

Fig. 20.6 DSC thermographs for a heating rate of 10 °C/min for (**a**) 63Sn-37Pb solder, (**b**) 63Sn-37Pb + 0.3 wt% SWCNT

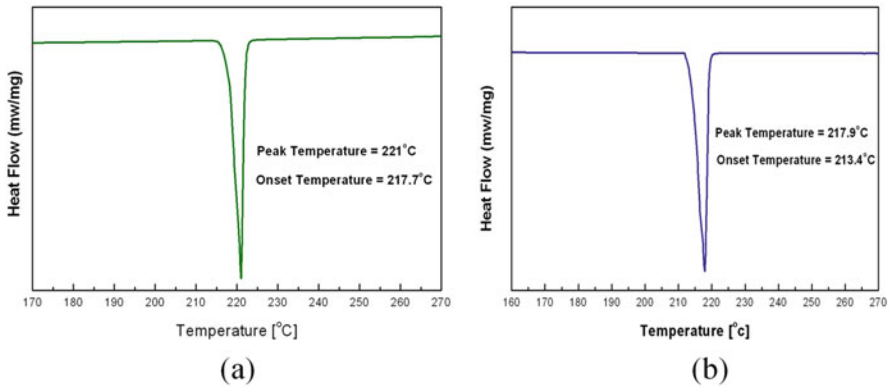

Fig. 20.7 DSC thermographs for a heating rate of 10 °C/min for (**a**) Sn-3.8Ag-0.7Cu (**b**) Sn-3.8Ag-0.7Cu +1 wt% SWCNT

20.3.3 Differential Scanning Calorimetry Analysis

DSC measurements were carried out to determine the thermal properties such as melting point and onset temperature of both Sn-Pb and Sn-Ag-Cu composite solders containing varying amounts of SWCNTs. The results are given in Table 20.1. Typical DSC thermograms of the Sn-Pb and Sn-Ag-Cu solders and their composites with SWCNTs are shown in Figs. 20.6 and 20.7. The shapes of the thermograms closely resemble one another. They are characterized by a sharp endothermic peak associated with the onset temperature and a peak temperature that exactly corresponds to the melting temperature of the solder or composite solder. It can be seen from Table 20.1 that the melting point of the composite solders as well as the onset

temperature decreases with increasing content of SWCNTs. A similar decreasing trend in melting point was recently reported for the addition of nano-alumina and nano-SiO_2 to polyether ether ketone (PEEK) [28].

The possible reasons for the reduction in melting point of solders could be due to the increase in the surface instability with the higher surface free energy rendered by the addition of SWCNTs. Also, the size effect of carbon nanotubes can significantly alter the grain boundary/interfacial characteristics of solders, resulting in such a change in physical properties [24, 29, 30].

It can be seen from Table 20.1 that both nanocomposite solders show decreasing melting points and onset temperatures with increasing nanotube content. However, the Sn-Ag-Cu/SWCNT system shows a much lower melting temperature than the Sn-Pb/SWCNT system. This was mainly attributed to the good adhesion between the nanotube and Ag_3Sn of the lead-free solder matrix.

Addition of SWCNTs has resulted in lowering the melting point of the Sn-Ag-Cu and Sn-Pb composite solders by only 3.4 °C and 1.5 °C, respectively. This lowering is not large, and the resultant nanocomposite solders can readily be adopted with the current recommended reflow conditions.

20.3.4 Electrical Conductivity

Figure 20.8 shows the variation of the electrical conductivity of the Sn-Pb and Sn-Ag-Cu composite solders with SWCNT wt%. The electrical conductivities of Sn-Pb and Sn-Ag-Cu solder are 10.58%IACS (International Annealed Copper Standard) and 14.29%IACS, respectively. It is evident from the graph that increasing the SWCNT content increases the electrical conductivity of the composite solders. The electrical conductivity of the Sn-Pb based composite solders increased from 10.58%IACS to 11.04%IACS with the addition of 0.05 wt% of SWCNTs. Further

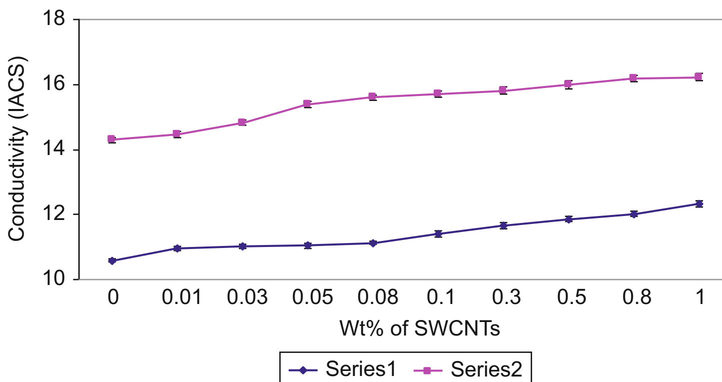

Fig. 20.8 Electrical conductivity of Sn-Pb and Sn-Ag-Cu composite solders versus SWCNT content

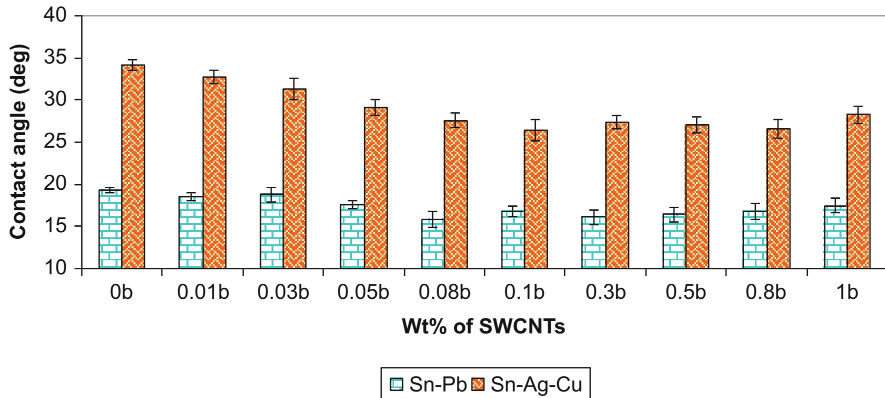

Fig. 20.9 Contact angles of composite solders on copper substrates with varying contents of SWCNT

addition of SWCNTs increased the conductivity value to 11.86%IACS. This increment is ~12% higher than the parent Sn-Pb alloy. A similar behavior is noted for the Sn-Ag-Cu-based composite solders. The room temperature conductivities of the bare Sn-Pb and Sn-Ag-Cu are comparable with those in the literature [27]. Similar increments in conductivity have been observed with epoxy nanotube composites [31].

The trend of increasing electrical conductivity of the nanocomposite solders with increasing amounts of SWCNT addition can be explained by the fact that at the percolation threshold, there is a network structure of nanotubes surrounded by the immobilized solder matrix. Even if the nanotubes do not touch each other, conductivity of the nanocomposites is increased as long as the distances between the tubes are lower than the hopping distance of the conducting electrons [32].

20.3.5 Contact Angle

Figure 20.9 shows the contact angles measured for both Sn-Ag-Cu and Sn-Pb solders as function of SWCNT content. As can be seen, the contact angle for both composite solders first decreases with SWCNT content up to about 0.1 wt% before increasing. The minimum value for Sn-Pb solder composite was 15.8° at 0.08 wt% SWCNT, while the minimum for Sn-Ag-Cu solder composite was 27° at 0.1 wt% SWCNT. The contact angle measured for Sn-Ag-Cu was 34.2°, which is very similar to the value reported by other researchers in the literature [27].

The effect of nanotube addition on the wettability can be explained as follows. An increase in the flux-copper surface energy, or decrease in flux-solder surface energy, will decrease the contact angle, thus increasing the wettability. SWCNT addition that

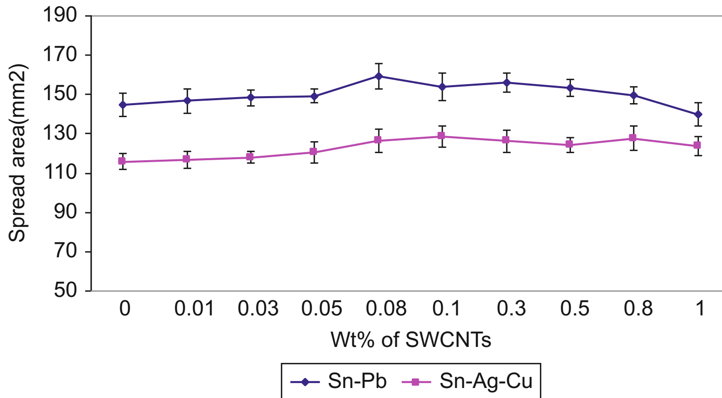

Fig. 20.10 Variations of the spreading area for composite solders with different wt% of SWCNT

promotes these changes will result in improved wettability. It is expected that increasing the SWCNT content to a certain extent could greatly increase the flux-solder surface tension because of chemical reactions. Similar findings have been reported by Loomans [33] for lead-free solder systems.

20.3.6 Wettability

The spreading area and wetting area of a fixed mass of solder were used to evaluate wettability [34]. Figure 20.10 shows the spreading area measured for both composite solders. This figure reveals a similar trend as the contact angle results. For both composite solders, the spreading area increases with SWCNT content up to about 0.1 wt% before decreasing. The maximum value for Sn-Pb solder composite was 159.5 mm^2 at 0.08 wt% SWCNT, while the maximum for Sn-Ag-Cu solder composite was 128.5 mm^2 at 0.1 wt% SWCNT.

It is believed that the addition of nanotubes enforced the orbital interaction between the tin atoms and the copper atoms and greatly improved the spreading area. However, further addition of nanotubes beyond a critical concentration deteriorated the wetting properties and reduced the spreading area of the composite solders. If there is a high level of nanotubes in the composite solder, tin atoms can no longer play the important role of base metal, since the orbital reaction between nanotubes and tin atoms is not strong. Therefore, the spreading area and wettability are worse with increasing levels of nanotubes beyond a certain critical value.

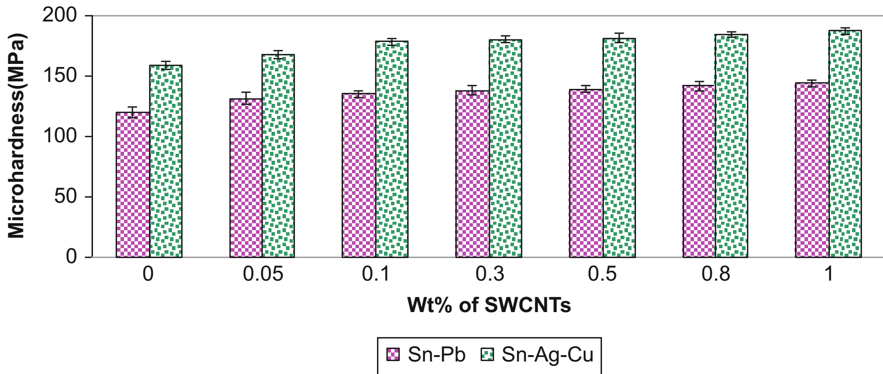

Fig. 20.11 Microhardness variation of the composite solders with different wt% of SWCNT

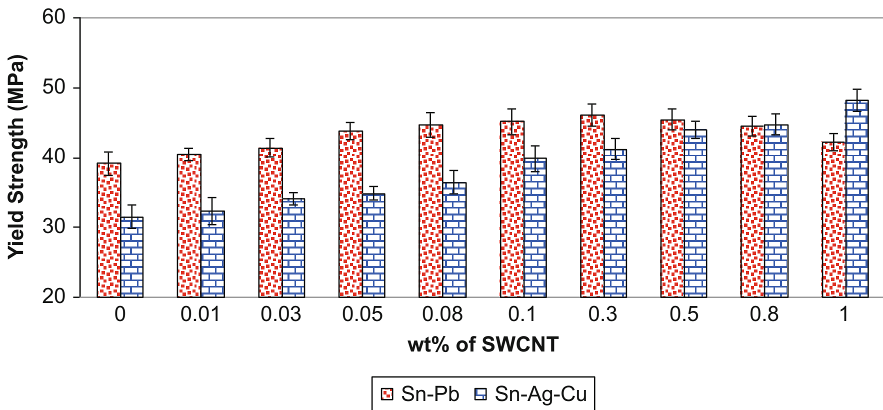

Fig. 20.12 Variations of yield strength of composite solders with wt% SWCNT

20.3.7 Microhardness

Figure 20.11 gives the microhardness values of the composite solder alloys as a function of SWCNT loading. Each value presented was obtained from an average of seven readings at different locations within each composite solder sample. A trend of increasing microhardness with SWCNT content was observed for both composite solder alloys. Microhardness tests show indeed that the SWCNT-reinforced Sn-Ag-Cu composite solders have slightly higher hardness than the SWCNT-reinforced Sn-Pb solder. The average microhardness of the Sn-Pb+0.5 wt% nanotube composite solder is approximately 16.5% higher than that of the Sn-Pb solder alloy, whereas 1 wt% addition of SWCNT to Sn-Ag-Cu solder resulted in nearly 18% improvement in the microhardness value as compared to the original Sn-Ag-Cu solder alloy.

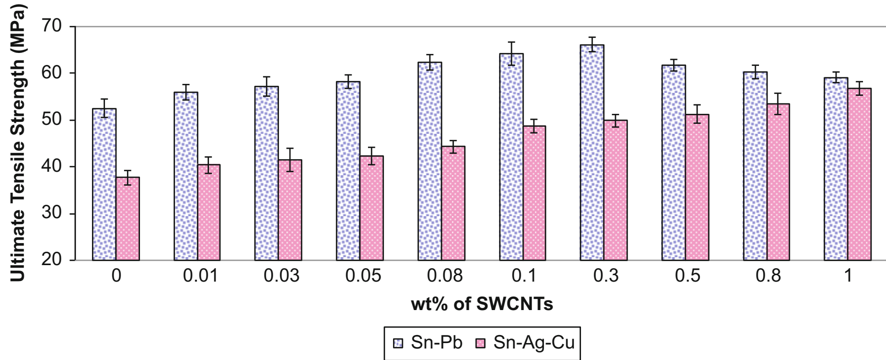

Fig. 20.13 Effect of SWCNT loading on UTS of Sn-Pb and Sn-Ag-Cu composite solders

20.3.8 Tensile Properties

20.3.8.1 Yield Strength

The influence of nanotube addition on the yield strength of both composite solders has been investigated and plotted in Fig. 20.12. It can be seen that the yield strength of both composites increases with the nanotube content. It is interesting to note that in the case of Sn-Ag-Cu composite solders, the yield strength increases continuously with nanotube content, while for Sn-Pb solders, the yield strength reaches a maximum value at 0.3 wt% of nanotube addition before decreasing. In both cases, it was found that it was impossible for the solders to absorb more than 1 wt% of SWCNT. The maximum increase in yield strength for Sn-Ag-Cu solder composite at 1 wt% of nanotube reinforcement was 52.9% higher than its pure counterpart, whereas the maximum increase in yield strength achievable for Sn-Pb solder was ~18% at 0.3 wt % of nanotube addition.

20.3.8.2 Ultimate Tensile Strength

Figure 20.13 shows typical variations of the ultimate tensile strength (UTS) of Sn-Pb-based composite solders in comparison with Sn-Ag-Cu-based composite solders as a function of different concentrations of SWCNTs. All the measured tensile strengths of nanocomposite solders exhibited very small deviations. The trends observed are similar to the effect of nanotube addition on the yield strength. The UTS of Sn-Ag-Cu solder specimens increase monotonically with increasing SWCNT, while the UTS of Sn-Pb reached a maximum at 0.03 wt% of SWCNT before declining. The maximum UTS of Sn-Pb-based composite solders achieved with the addition of 0.3 wt% of SWCNTs was ~26% higher than undoped Sn-Pb solder. The effect of SWCNT on the UTS of solder is similar to its effect on polymers [31]. A maximum increase of about ~51% was observed for the Sn-Ag-Cu solder. The improvement in the tensile strength may be caused by the strong

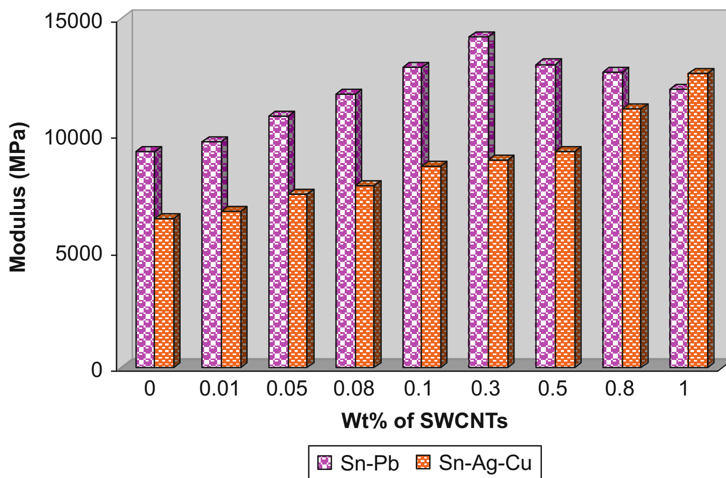

Fig. 20.14 Variation of the tensile modulus of composite solders with wt% SWCNT

interactions between the solder matrix and the SWCNTs, which leads to good dispersion of SWCNTs in the nanocomposites. These well-dispersed SWCNTs may be the reason for the increase in the tensile strength. However, when the content of SWCNT is too high, the SWCNTs cannot be properly dispersed in the solder matrix and agglomerate into clusters because of the huge surface energy of SWCNTs [35, 36]. This probably caused the decrease of tensile strength as observed in the case of Sn-Pb solder doped with more than 0.3 wt% nanotube.

20.3.8.3 Tensile Modulus

The variation of tensile modulus of both composite solders (Sn-Pb and Sn-Ag-Cu) with wt% reinforcement of SWCNT is shown in Fig. 20.14. As with the yield strength and UTS, the tensile modulus for Sn-Ag-Cu composite solder increases monotonically with wt% reinforcement of SWCNT while that for Sn-Pb has a maximum at 0.3 wt%. The general increase of tensile modulus with %wt SWCNT is probably due the reinforcing effect imparted by the nanotubes that allowed a greater degree of stress transfer at the grain boundaries. A possible explanation can be given for the behavior for Sn-Pb composite solders by assuming a similar state of high-quality dispersion for all nanocomposites after the sintering process. An increasing amount of agglomerates in the sintered composite was observed for the SWCNT/Sn-Pb solder composites with nanotube content above 0.3 wt%. We propose these agglomerates to be a result of re-agglomeration which reduces the Young’s modulus more significantly. The largest modulus of Sn-Ag-Cu composite solder was 12,642 MPa at 1 wt% SWCNT, which is almost 98% higher than the value of 6385 MPa for the original solder. The largest modulus for Sn-Pb composite

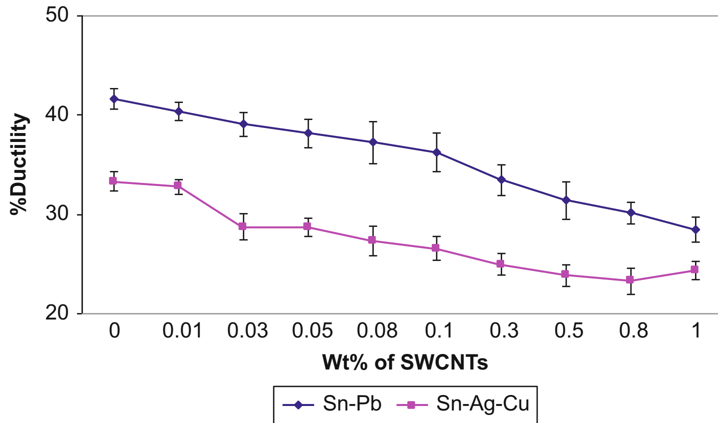

Fig. 20.15 Ductility of nanocomposite solders as a function of SWCNT content

solder was 14,216 MPa at 0.3 wt% CNT, which represents an increase of 53% over the value of 9276 MPa for the original solder.

20.3.8.4 Ductility

Ductility was quantified by measuring the plastic strain to failure. Appreciable ductility was measured for both Sn-Pb and Sn-Ag-Cu composite solders. A plot of ductility (% elongation) as a function of SWCNT loading is shown in Fig. 20.15. The tests demonstrated a downward trend of % elongation with increase in the SWCNT content for both composite solders. Sn-Ag-Cu solder shows a 33.3% elongation at break. Almost 26.6% elongation at break was found for 0.1 wt% of SWCNT added. The elongation to failure was observed to be 23.8% at the 1 wt% of SWCNT addition, which is ~27% lower than the virgin Sn-Ag-Cu solder matrix. This indicates that adding the nanotubes to Sn-Ag-Cu solder material increases brittleness which is consistent with the previous studies of composite solders reported by Chen et al. [36]. As shown in Fig. 20.15, the % elongation of 0.03 wt % reinforced Sn-Pb solders was obviously lower than those of pure Sn-Pb solder; the elongation decreases with increasing SWCNT content from 0.03 to 0.5 wt%. At 0.5 wt% SWCNT, the ductility is ~24% lower than the Sn-Pb solder. From this it is evident that both composite solders showed an increase in brittle characteristics due to the rigidity of the composite solder matrix as SWCNT content increased. In all the cases, the elongation to failure decreases. The major reason is that SWCNTs included into the solder matrix behave like physical constraints and restrict the deformation of the solder matrix.

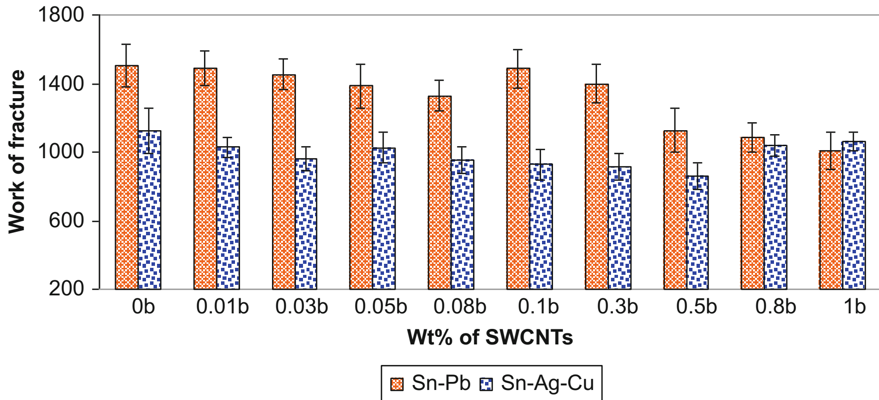

Fig. 20.16 Influence of SWCNT content on the work of fracture of Sn-Pb and Sn-Ag-Cu composite solders

Table 20.2 Grain sizes of the Sn-Pb and Sn-Ag-Cu composite solders

Solder alloy	Grain size (μm)
63Sn-37Pb	5.12
63Sn-37Pb + 0.3 wt% CNT	1.08
Sn-3.8Ag-0.7Cu	3.75–4.25
Sn-3.8Ag-0.7Cu + 1 wt% SWCNT	0.5–0.8

20.3.8.5 Work of Fracture

Figure 20.16 shows a plot of the work of fracture versus the various SWCNT loading for the Sn-Pb and Sn-Ag-Cu composite solders. However, the work of fracture of Sn-Ag-Cu composite solders did not vary linearly with increase in SWCNT content. Maximum and minimum values were observed in this case. The minimum work of fracture was observed at 0.5 wt% addition of SWCNT, while the maximum was observed for the undoped Sn-Ag-Cu solder. For Sn-Pb solder, the minimum work of fracture occurred at 0.8 wt% CNT, while the maximum was observed for the undoped Sn-Pb solder.

20.3.9 Strengthening Mechanisms

20.3.9.1 Grain Size Refinement

Table 20.2 gives the grain size values measured using image analysis for both composite solders with and without reinforcement of nanotubes. As is common in composite materials, the grain size decreases as the weight fraction of reinforcement addition increases. Since nanotubes may act as nucleation sites for recrystallized grains during sintering, the volume fraction of recrystallization grains increases

when the reinforcement volume fraction increases; it can be observed that, as the weight fraction of the SWCNT rises, the grain size of the composite solder diminishes, causing strengthening by the Hall-Petch mechanism. SWCNTs control the grain size of the composite solders, since they prevent grain growth. This grain size refinement can be clearly seen in the microstructure of the composite solders shown in Fig. 20.3. The Hall-Petch relation can be formulated as

$$\sigma_H = \sigma_o + \frac{k}{\sqrt{D}},$$

where

σ_H = yield stress
σ_o = friction stress
k = constant
D = grain size

The yield stress increases as the grain size of the composite diminishes.

20.3.9.2 CTE Mismatch

63Sn-37Pb solder has a coefficient of thermal expansion of 25.8×10^{-6}/°C, while SWCNTs exhibit a much lower coefficient of thermal expansion of -1.5×10^{-6}/°C [35]. Hence, in the SWCNT-doped Sn-Pb solders, there exists a significant CTE mismatch between the SWCNT reinforcement and the solder matrix. This CTE mismatch can result in the prismatic punch of the dislocations at the interface which in turn can lead to the work hardening of the solder matrix. The dislocation density that is generated due to the CTE mismatch between the reinforcement and the solder matrix is directly proportional to the surface area of the reinforcement. The diameter of a SWCNT is very small leading to a lower density of Griffith flaws. Due to the lower Griffith flaws, the number of dislocations generated is likely to be higher, which in turn could result in the increased strengthening effect.

The dislocation density can be formulated as

$$\rho^C = \frac{10A\varepsilon f_{SWCNT}}{(1 - f_{SWCNT})bd_{SWCNT}}$$

where f_{SWCNT} is the weight fraction of the SWCNTs, ε is the misfit strain due to the difference in the CTE values of SWCNT and solder matrix, b is the Burgers vector, and d_{SWCNT} is the diameter of the SWCNT.

The increment in stress can be indicated by

$$\Delta\sigma_C = \sqrt{3\alpha\mu b}\sqrt{\rho^C},$$

where

μ= modulus of rigidity of the solder
b= Burgers vector
α = constant

20.3.9.3 Orowan Mechanism

The interaction between the dislocations and the SWCNTs can inhibit the motion of the dislocations, leading to bending of the dislocations between the nanotubes. Bending of dislocations produces a back stress, which could prevent further dislocation migration and result in an increase in yield stress. The Orowan mechanism is less significant in the metal matrix composites where the reinforcements are generally coarser in shape and the interparticle spacing is large, but it is more effective in the SWCNT-reinforced composites as the nanotubes effectively represent the fine particles having very narrow diameters of the order of a few nanometers. In this manner SWCNT can effectively strengthen the solder matrix by interacting with the dislocations.

Thus the increment in the shear strength of the composite solders can be written as

$$\Delta\tau = K^{*}\mu A^{1/2} b/r^{*} \ln\left(2r/r_{o}\right),$$

where

K = a constant characterizing the transparency of the dislocation forest for basal-basal dislocation interaction
μ = modulus of rigidity of the solder matrix
r = volume equivalent radius of SWCNT = 7.087 nm
b = Burgers vector
A = constant = 0.093 for edge dislocations and 0.14 for screw dislocations

20.3.9.4 Residual Stresses

The CTE mismatch between the nanotubes and solder matrix resulted in the presence of residual stresses in the composite solder. The solder matrix remains in tension and the reinforced nanotubes in compression. A similar situation was observed when the metal matrix composites are reinforced with ceramic reinforcements [37]. Presence of residual stresses can also lead to the increment in the yield stress of the composite solders.

It is possible to conclude from the above discussion that the increment in yield strength and ultimate tensile strength of the composite solders has three main contributions: the grain size refinement, increase in dislocation density due to the CTE mismatch between the solder matrix and nanotubes, and the Orowan looping mechanism.

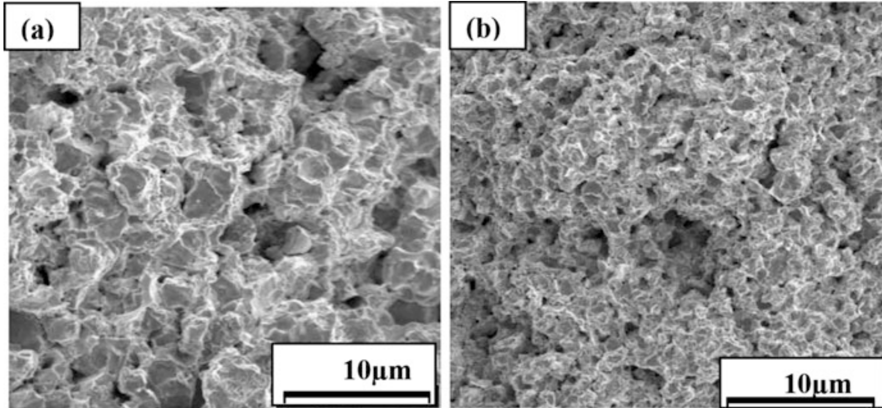

Fig. 20.17 Low magnification FE-SEM micrographs of the fracture surfaces of the Sn-Pb solder composite specimens with (**a**) 0.01 wt%, (**b**) 0.5 wt% SWCNT

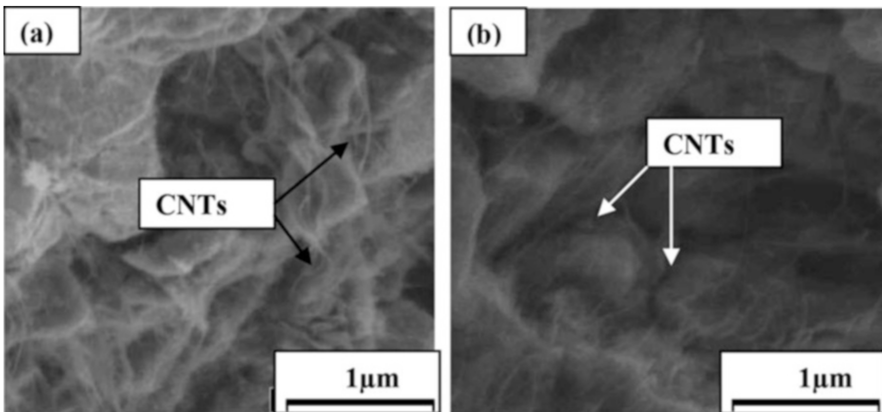

Fig. 20.18 High magnification FE-SEM fractographs of Sn-Pb composite solders with (**a**) 0.01 wt %, (**b**) 0.5 wt% SWCNT

The decrease in ductility of the composite solders can be explained by the following mechanism. The reduction of ductility, with the higher reinforcement addition, is a very common phenomenon observed in metal matrix-based composites [38, 39]. The main reason may be the limited ductility exhibited by SWCNTs [40]. In addition, the SWCNTs may restrict the movement of dislocations either by inducing the large difference in the elastic behavior between SWCNTs and the matrix or creating the stress fields around the dislocations.

20.3.10 Fracture Studies

Fracture surfaces of Sn-Pb composites are shown in Fig. 20.17a, b. The lower magnification topographies which are represented indicate extreme ductile fracture modes, characterized by dimples on the surface. Closer observations at higher magnifications shown in Fig. 20.18a, b demonstrated the breakage of nanotubes.

Figure 20.17a shows the fractograph of the Sn-Pb solder specimens. The fracture surface shows evidence of high ductility with the dimples. However, the composite solders reinforced with nanotubes exhibited a limited ductility; the fracture occurred normal to the loading axis as is shown in Figs. 20.17 and 20.18. Figure 20.18 indicates that after tensile deformation, the solder matrix adheres well to the nanotubes due to the highly ductile nature of the matrix alloy. Dimples were observed on the composite solder surfaces in the region between the nanotubes and solder matrix. The nanotubes appeared to have been cut at the surfaces. From this observation, it can be inferred that the fracture took place in the solder matrix by void generation and propagation, finally resulting in the shearing of the nanotubes adhered to the matrix. This indicates that strong interface bonding has been developed in the nanotube-reinforced solder composites.

20.3.10.1 Fracture Mechanism for Sn-Pb Composite Solders

It is evident from the fractographs shown in Fig. 20.18 that the direction of the internal cracks in the composites is normal to the tensile loading axis. Here no nanotube pull-outs were observed. According to these findings, it is noted that the crack was initiated in the solder matrix and then propagated and sheared through the nanotube reinforcements. These findings are consistent with the strong interfacial bonding between the solder matrix and the nanotubes.

According to Lloyd [38, 39], there are three possible ways that fracture behavior can be observed in composite materials. (1) If the interface between the reinforcement and the matrix is weak, the crack can initiate and can propagate through the interface. (2) If the interface and the matrix are both strong, the reinforcement can be loaded up to the fracture stresses and then be cracked. (3) If the matrix is weaker than the interfacial and reinforcement strengths, the fracture may occur in the matrix by void coalescence and growth mechanism. In the present SWCNT-based composites, the fracture mechanism observed can be described as follows. The fracture probably initiated in the relatively weaker solder alloy matrix rather than at the solder-nanotube interface or in the nanotube. The fracture can be initiated by void nucleation and propagation. When the crack reaches the nanotube-solder matrix interface, the nanotube-solder matrix interface does not separate due to the high interfacial bonding. Consequently high stresses will be developed at the nanotubes causing them to be sheared off when their failure stress is reached.

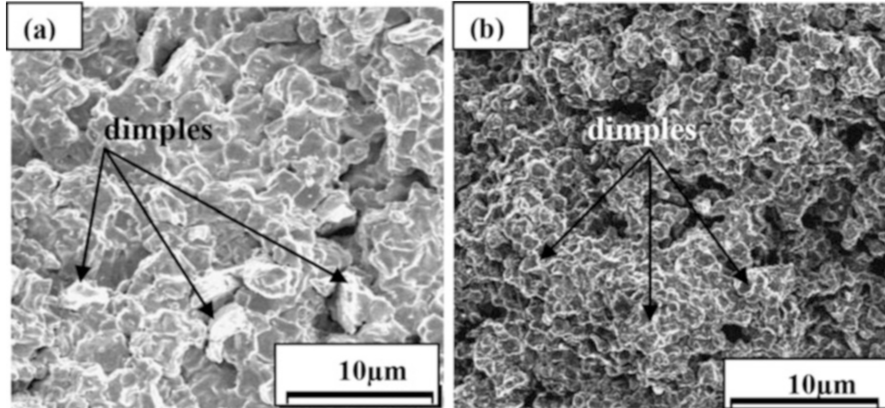

Fig. 20.19 Low magnification FE-SEM micrographs of the fracture surfaces of the Sn-Ag-Cu composite solder specimens with (**a**) 0.01 wt%, (**b**) 1 wt% SWCNT

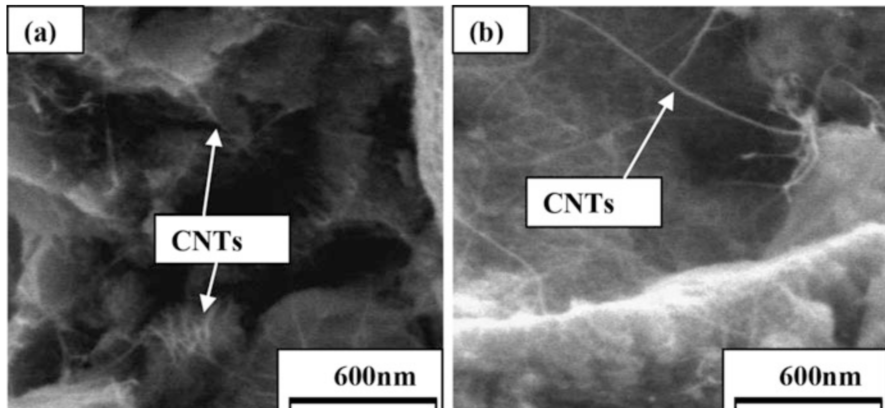

Fig. 20.20 High magnification FE-SEM micrographs of the fracture surfaces of the Sn-Ag-Cu composite solder specimens with (**a**) 0.01 wt%, (**b**) 1 wt% SWCNT

20.3.10.2 Fracture Mechanism for Sn-Ag-Cu Composite Solders

The detailed fracture behavior of Sn-Ag-Cu composite solder specimens were revealed by extensive fractographic observations. Scanning electron microscopy was performed at high magnification to probe the fractured specimens that were deformed during tensile loading. Typical FE-SEM micrographs of fracture surfaces at lower magnification with the various additions of nanotubes are shown in Fig. 20.19. As can be seen in Fig. 20.20, the fractured surfaces of the composite specimens mainly consist of matrix dimples and fractured nanotubes. These observations are consistent with those reported in the literature where MWCNTs were employed [41]. From the fractured surface, it is observed that SWCNTs are

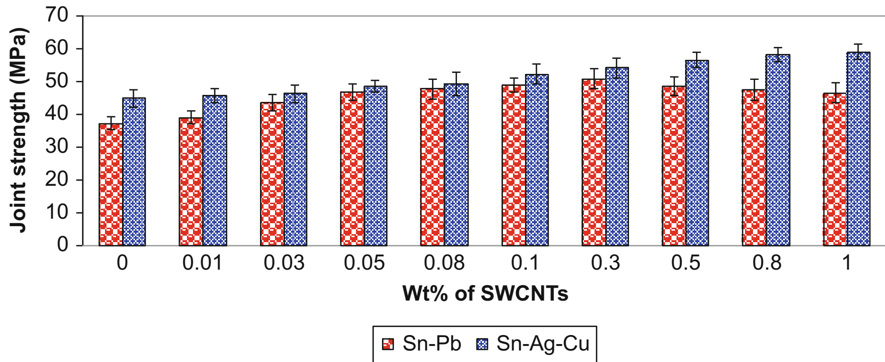

Fig. 20.21 Tensile joint strength values of Sn-Pb and An-Ag-Cu composite solders as functions of wt% of SWCNT

vertically aligned to the fracture surface during the tensile deformation of the composite solder specimens and this alignment might be one of the reasons for the increase in the strength of the composite solders. A similar effect has been observed in SiO_2-based CNT composites [42].

Figure 20.20 shows that cracks run through the SWCNTs that remain in the matrix of the solders. It is evident that fracture occurred mostly by the failure of the matrix and not by the debonding of the interface between SWCNT and solder matrix. There is some evidence of partial debonding at the interface between Ag_3Sn and the lead-free solder matrix, but none at the interface between SWCNT and the solder matrix.

Because of the high aspect ratio of SWCNTs, micro cavities may form at the ends, and this is one of the ways micro cavities are formed inside the matrix. From Fig. 20.3, it is clear that Ag_3Sn has the equiaxed grain shape, compared to SWCNTs. As the deformation increases, the micro cavities that already exist in the matrix grow parallel to the tensile loading axis, and the deformation becomes localized into intense shear deformation zones in which the Ag_3Sn grains can be completely debonded to form voids. Subsequently, these voids in the shear deformation zones combine with the micro cavities at the ends of the SWCNTs to cause the failure of the solder matrix. Final failure occurs through the breakage of the SWCNTs.

20.3.11 Solder Joint Strength with Copper Substrate

Figure 20.21 illustrates the influence of the nanotube addition on Cu-solder-Cu joint strength under tensile loading conditions. It can be seen that the strength of the solder joints increased after the incorporation of nanotubes into the solder alloys. For Sn-Ag-Cu solder, the strength of the joint increased monotonically with the content of SWCNTs. The joint strength at 1 wt% was 59.1 MPa, approximately 32% higher

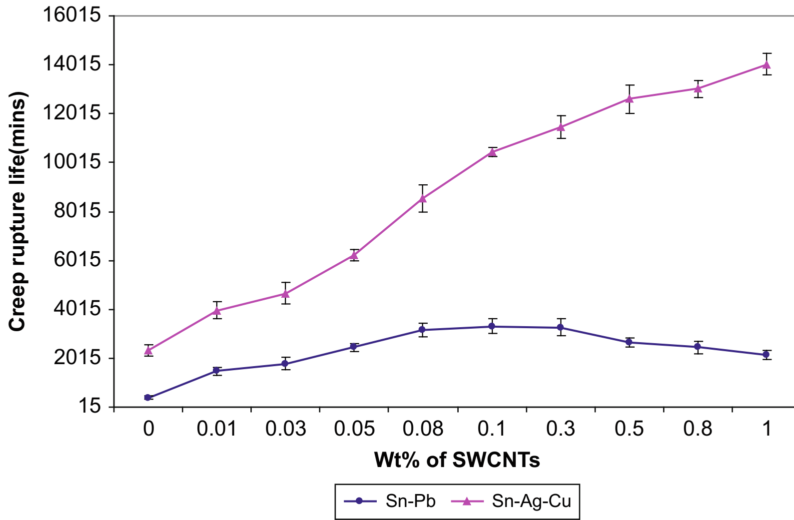

Fig. 20.22 Creep rupture times of the Sn-Pb and Sn-Ag-Cu composite solders as a function of wt% SWCNT

than the value for the undoped Sn-Ag-Cu solder. For Sn-Pb composite solders first increased with SWCNT content, reached a maximum, and then decreased. The maximum joint strength reached was 50.8 MPa with 0.3 wt% SWCNT, which was approximately 37% higher than the undoped Sn-Pb solder.

20.3.12 Creep Rupture Analysis

The creep rupture life of both Sn-Pb and Sn-Ag-Cu composite solders as a function of SWCNT content is presented in Fig. 20.22. Creep rupture life of both composites increased with increasing SWCNT content. In the case of Sn-Ag-Cu composite solders, the increase is monotonic, reaching a value of 14,043 min with a SWCNT content of 1 wt% which is about six times the creep rupture time for the undoped Sn-Ag-Cu solder. In the case of Sn-Pb composite solders, however, the creep rupture time first increases, reaches a maximum at 0.1 wt% CNT, and then decreases with further increase of SWCNT content. The maximum creep rupture life attained for Sn-Pb composite solder was 3324 min which is 8.29 times higher than the value for the undoped Sn-Pb solder.

20.4 Conclusions

The goal of this work was to produce and characterize novel SWCNT-reinforced composite solders for fine-pitch wafer-level packaging applications. Composites of Sn-Pb and Sn-Ag-Cu solders and SWCNTs were prepared by a sintering process. Microstructural studies of the composite solders confirmed the uniform and homogenous distribution of nanotubes in the solder matrix. Nanotube addition also resulted in grain refining. CTEs of the composite solders were found to decrease with increasing weight content of nanotubes. It was found that the melting point of composite solders was lowered with increasing content of SWCNT but the decrease is not substantial and can readily be integrated with existing manufacturing conditions. The contact angles and wettability of composite solders on copper substrates were studied. Among the solders tested, Sn-Pb + 0.08% SWCNT and Sn-Ag-Cu + 0.1% SWCNT exhibited the lowest contact angle and highest spreading area, indicating excellent wettability. Microhardness values improved with the amount of nanotube addition for both the composite solders due to homogenous dispersion of nanotubes throughout the solder matrix. Mechanical properties such as modulus, yield strength, and ultimate tensile strength showed improvement with the nanotube addition. It was found that for Sn-Ag-Cu solder, the improvement in mechanical properties increased monotonically with SWCNT content, while for Sn-Pb solder, the improvement first increased and reached a maximum before decreasing. SEM fractographs of the composite solder specimens revealed the ductile fracture mode of the composites, which is characterized by dimples. The addition of nanotubes significantly improved the creep rupture life of both Sn-Pb and Sn-Ag-Cu composite solders.

References

1. International Technology Roadmap for Semiconductors-Assembly and Packaging (2003) http://public.itrs.net/Files/2003 ITRS/Home 2003.html
2. Tummala RR (2001) Fundamentals of microsystems packaging. McGraw Hill, New York
3. Yeth CC, Choi WJ, Tu KN (2002) Current-crowding-induced electromigration failure in flip chip solder joints. Appl Phys Lett 80:580
4. Lau JH (1997) Flip chip technologies. McGraw Hill, New York
5. Stam FA, Davitt E (2001) Effects of thermomechanical cycling on lead and lead-free (SnPb and SnAgCu) surface mount solder joints. Microelectron Reliab 41:1815
6. Mavoori H, Jin S (1998) New, creep-resistant, low melting point solders with ultrafine oxide dispersions. J Electron Mater 27:1216
7. Reno RC, Panunto MJ (1997) A Mössbauer study of tin-based intermetallics formed during the manufacture of dispersion-strengthened composite solders. J Electron Mater 26:11
8. Chen K-I, Lin K-L (2002) The microstructures and mechanical properties of the Sn-Zn-Ag-Al-Ga solder alloys—the effect of Ag. J Electron Mater 31:861
9. Nai SML, Wei J, Gupta M (2006) Improving the performance of lead-free solder reinforced with multi-walled carbon nanotubes. Mater Sci Eng A423(1–2):166–169
10. Ijama S (1991) Helical microtubules of graphite carbon. Nature 354:56–58

11. Lu JP (1997) Elastic properties of carbon nanotubes and nanoropes. Phys Rev Lett 79:1297–1300
12. Saether E, Frankland SJ, Pipes RB (2003) Transverse mechanical properties of single-walled carbon nanotube crystals. Part I: determination of elastic moduli. Compos Sci Technol 63:1543
13. Despres JF, Daguerre E, Lafdi K (1995) Flexibility of graphene layers in carbon nanotubes. Carbon 33:87–92
14. Iijima S, Brabec C, Maiti A, Bernholc J (1996) Structural flexibility of carbon nanotubes. J Phys Chem 104:2089–2092
15. Dai H, Wong EW, Lieber CM (1996) Probing electrical transport in nanomaterials: conductivity of individual carbon nanotubes. Science 272:523–526
16. Ebbesen TW, Lezec HJ, Hiura H, Benett JW, Ghaemi HF, Thio T (1996) Electrical conductivity of individual carbon nanotubes. Nature 382:54–56
17. Yakobson BI, Brabec CJ, Bernholc J (1996) Nanomechanics of carbon tubes: instabilities beyond linear response. Phys Rev Lett 76:2511–2514
18. Salvetat-Delmotte J, Rubio A (2002) Carbon 40:1729
19. Zhong R, Cong H, Hou P (2003) Mechanical properties of carbon nanotubes: a fiber digest for beginners. Carbon 41:848
20. Dong S, Zhang X (1999) Mechanical properties of Cu-based composites reinforced by carbon nanotubes. Trans Nonferrous Meter Soc China 9:457
21. George R, Kashyap KT, Rahul R, Yamdagni S (2005) Strengthening in carbon nanotube/aluminium (CNT/Al) composites. Scr Mater 53:1159–1163
22. Peigney E, Laurent C, Flahaut A, Rousset A (2000) Carbon nanotubes in novel ceramic matrix nanocomposites. Ceram Int 26:677–683
23. Xu CL, Wei BQ, Ma RZ, Liang J, Ma XK, Wu DH (1999) Fabrication of aluminum–carbon nanotube composites and their electrical properties. Carbon 37:855–858
24. Couchman PR, Ryan CK (1978) The Lindmann hypothesis and the size-dependence of melting temperature. Philos Mag A 37:327–329
25. Upadhya K (1993) Proceedings of a symposium sponsored by the structural materials division of TMS annual meeting, Denver, p 22
26. Wu WF, Lin YY, Young HT (2005) Quantitative reliability analysis of electronic packages in consideration of variability of model parameters, Proceedings of 7th electronics packaging technology conference, Singapore, EPTC2005, p 625
27. NIST solder data base. http://www.boulder.nist.gov/div853/lead%20free/solders.html
28. Kuo MC, Tsai CM, Huang JC, Chen M (2005) PEEK composites reinforced by nano-sized SiO2 and Al2O3 particulates. Mater Chem Phys 90:185–195
29. Lindemann FA (1910) Phy Z 11:609–617
30. Ziman JM (1972) Principles of the theory of solids. Cambridge University Press, London
31. Sandler JKW, Kirk JE, Kinloch IA, Shaffer MSP, Windle AH (2003) Ultra-low electrical percolation threshold in carbon-nanotube-epoxy composites. Polymer 16(3):248–251
32. Potschke P, Abdel-Goad M, Alig I, Dudkin S, Lellinger D (2004) Rheological and dielectrical characterization of melt mixed polycarbonate-multiwalled carbon nanotube composites. Polymer 45:8863
33. Loomans ME, Vaynman S, Ghosh G, Fine ME (1994) Investigation of multi-component lead-free solders. J Electron Mater 23:741
34. Werner E (2006) A guide to lead-free solders physical metallurgy and reliability. Springer, London
35. Ruoff RS, Lorents DC (1995) Mechanical and thermal properties of carbon nanotubes. Carbon 33(7):925–930
36. Chen Z, Yaowu S, Xia Z, Yan Y (2003) Properties of lead-free solder SnAgCu containing minute amounts of rare earth. J Electron Mater 32:235
37. Gojny FW, Wichmann MHG, Fiedler B, Schulte K (2006) Compos Sci Technol 66:343–349
38. Lloyd DJ (1994) Particle reinforced aluminium and magnesium matrix composites. Int Mater Rev 39:1–23

39. Lloyd DJ (1997) Processing of particle-reinforced metal matrix composites. In: Mallick PK (ed) Composite engineering handbook. Marcel Dekker, New York, pp 631–670
40. Cadek M, Coleman JN, Barron V, Hedicke K, Blau WJ (2002) Morphological and mechanical properties of carbon-nanotube-reinforced semicrystalline and amorphous polymer composites. Appl Phys Lett 81(27):5123–5125
41. Lloyd DJ, Lagace HP, McLeod AD (1990) Interfacial phenomena in metal matrix composites. Proceedings of ICCI-III. Elsevier, Cleveland, pp 359–376
42. Ning J, Zhang J, Pan Y, Guo J (2003) Fabrication and mechanical properties of SiO2 matrix composites reinforced by carbon nanotube. Mater Sci Eng A 357:392